EUROPEAN ORGANIZATION FOR NUCLEAR RESEARCH

CERN-EP/80-86
3 June 1980

FISSION OF ^{232}Th AND ^{238}U IN THE INTERACTION WITH NEGATIVE MUONS

Dz. Ganzorig[a)], P.G. Hansen[b,1)], T. Johansson[b,2)], B. Jonson[b,3)], J. Konijn[b,4)], T. Krogulski[c)], S.M. Polikanov[b)], G. Tibell[b,5)], and L. Westgaard[d)]

ABSTRACT

Muon induced fission of ^{232}Th and ^{238}U was studied, measuring the time correlation between stopping muons, fission events and electrons.

The measured muon lifetimes are τ_μ (^{232}Th) = (77.3 ± 0.3) ns and τ_μ (^{238}U) = = (77.1 ± 0.2) ns. After prompt fission the muon was found to be attached predominantly to the heavy fragment with a lifetime for ^{232}Th of (132 ± 7) ns and for ^{238}U of (134 ± 4) ns. The probability for muon conversion was found to be a few percent per fission event.

Indications were found that the muonic shape isomer is populated in ^{238}U when the nucleus is excited in a radiationless muonic transition.

(Submitted to Nuclear Physics A)

a) Joint Institute of Nuclear Research, Dubna, USSR.
b) CERN, Geneva, Switzerland.
c) Institute of Nuclear Research, Swierk, Poland.
d) Department of Chemistry, University of Oslo, Norway.

1) Now at the Institute of Physics, University of Aarhus, Aarhus, Denmark.
2) On leave from the Gustaf Werner Institute, Uppsala, Sweden.
3) On leave from the Department of Physics, Chalmers University of Technology, Göteborg, Sweden.
4) Now at IKO, Amsterdam, the Netherlands.
5) Now at the Gustaf Werner Institute, Uppsala, Sweden.

1. INTRODUCTION

The interaction fissile nuclei with negative muons has been studied since the sixties [1-19]. Among other things, these investigations confirmed Wheeler's predictions [20] that there should be two different processes leading to fission of heavy nuclei in the interaction with μ^-. The first and most frequent is the fission of a nucleus excited by nuclear muon capture. The time distribution of such fission events is characterized by a mean life of about 80 ns, typical for muon capture in heavy elements. The second process leading to fission occurs in prompt coincidence with the stopping muons. It was interpreted as being due to nuclear excitation caused by muonic radiationless transitions. This process takes place with the nucleus surrounded by a muon in its 1s orbit, i.e. we are concerned with the fission of muonic atoms. For the heavy elements the muon in this orbit deeply penetrates the nucleus, spending more than half of its time inside the nuclear volume. The binding energy of the muon in the 1s orbit ($\sim$ 12 MeV) depends appreciably on the nuclear deformation, and thus the presence of the muon strongly influences the fission barrier.

This has interesting consequences for a double-humped barrier. Simple calculations give an isomer shift of about 0.5 MeV [21] when the heights of the first and second barriers are increased by 0.1 and 1.0 MeV, respectively. An experimental determination of the changes in the properties of the known isomeric states would be complementary to the proof already obtained from other experiments [22] that this state is a *shape* isomer [23].

The subsequent fate of the muon after it has induced fission is of interest from the point of view of fission dynamics [24-26]. The ratio of muons following the heavy and light fragments, respectively, may yield information on the time scale for the motion of the fissioning nucleus between saddle and scission points. A study of the fate of the muon might also give information on the muon conversion process, charge distributions in neutron-rich nuclei (fission fragments), etc.

We report here on an experiment where we have measured the time correlation between the incident muon, the induced fission event, and the electron from the muon beta-decay in ^{232}Th and ^{238}U. This method has the advantage of suppressing the strong background from μ^- capture by more than a factor of 100, and of making possible a search for i) muonic shape-isomer decay, ii) bare-nucleus shape-isomer decay, and iii) the fate of the muon after fission.

The main interest of the present measurements was the fission of muonic atoms. However, various aspects of fission due to muon capture have to be dealt with. There are, for instance, considerable discrepancies in the experimental determinations of the probability of muon-induced fission [4,14,17], and this point should be further investigated.

Some of the results from the present experiment have already been published; namely, on the disappearance rates of muons as observed in the fission mode [13], and on the fate of the muons after fission events which occur in prompt coincidence with the stopping muons [12]. The question of muonic shape-isomer excitation is discussed below in sections 3 and 4, and our results are compared with those of some other groups who have reported on this subject. In one of the published articles [9] weak indications are given that such an excitation has been observed.

Before the discussion of our results, we give a detailed account of the experimental equipment, as well as various checks and procedures. In section 3 the data evaluation procedure is described and the results are presented.

2. EXPERIMENTAL DETAILS

2.1 Beam and detectors

The experiment was performed at the muon channel of the CERN Synchro-cyclotron. With the accelerator operating in the normal sharing mode, the muon beam intensity was of the order of 20,000 s^{-1}. This number was obtained as the rate of double coincidences between the first two counters in the muon telescope (see fig. 1). The beam dimension was defined by a circular lead collimator in the wall and a likewise circular lead collimator placed between counters 1 and 2. During optimum

running conditions the microscopic duty cycle was about 60% with no noticeable macroscopic pulsing. The muon momentum was about 110 MeV/c. The π^- and e^- admixtures were on the level of 1% and 10%, respectively. The primary pion beam, with a momentum of about 200 MeV/c, was used for the tests described below.

The muon telescope consisted of two plastic scintillation counters, a plexiglas Čerenkov counter used to veto beam electrons as well as secondary electrons originating in the graphite moderator, and a final circular plastic scintillation counter. The inclusion of the third plastic counter reduced the (12) coincidence rate by typically 30%, and the whole telescope rate ($12\bar{C}3$) was a little over 50% of the primary beam rate as defined by the (12) coincidences. A conventional stop counter was not used; instead, the stop rate was maximized by using the muon-fission coincidence rate. Figure 1 gives a schematic view of the experimental configuration.

The fission chamber served as both target and detector with the fissile material (natural thorium or uranium) deposited on 100 aluminium foils, each 0.01 mm thick. These were separated by 2 mm and formed the electrodes of a parallel-plate, fast ionization chamber, divided into five independent sections. With a total weight of approximately 25 g, the target material had a thickness in the beam of about 600 mg/cm^2. The chamber walls were made of aluminium, and the chamber was filled with methane to a pressure of 2 ato. Some of the characteristic properties measured with the beam are shown in fig. 2. The efficiency for the threshold position indicated in fig. 2 was (38 ± 4)% using Segrè's value [27] for the spontaneous fission decay rate of ^{238}U. In the course of the experiment the time resolution for prompt (π,f) coincidences was checked many times and found to be very stable (4.5 ± 0.5) ns (FWHM).

The electron detector consisted of cylindrical plastic scintillation counters placed around the fission chamber with a Čerenkov counter outside the plastic counters. Two different Čerenkov counters were used: one consisting of a water tank, made in the form of a box with a central hole for fission chamber plus one cylindrical plastic counter, and the other made of four separate semicylindrical

plexiglas counters. In the latter case two concentric, cylindrical plastic counters were placed inside the Čerenkov counter. Consequently, two versions of the electron detector were used:

i) water tank $\check{C}$ counter with 5 cm thick walls working in coincidence with a cylindrical plastic scintillation counter of 0.9 cm thickness; and

ii) semicylindrical plexiglas $\check{C}$ counters of 2.5 cm thickness and two cylindrical plastic scintillation counters, 0.9 and 0.5 cm thick, respectively. This version of the electron detector was operated with either only the inner ("double mode") or both ("triple mode") of the scintillation counters in coincidence with the Čerenkov counter.

Taking into account the amount of material an electron originating in the centre of the fission chamber had to traverse, there was a threshold for detection at about 10 MeV in the electron energy.

2.2 Electronics and data acquisition system

With the detector system described above, fast timing signals were obtained corresponding to i) the arrival of a muon, defined by the third counter in the telescope, ii) a fission event occurring in any one of the five sections of the fission chamber (logic sum), and iii) the arrival of an electron, defined by one of the cylindrical scintillation counters. Using time-to-digital converters (TDCs), three time intervals were measured: $t(\mu,f)$, $t(\mu,e)$, and $t(f,e)$ in the time ranges 500 ns, 5 μs, and 5 μs, respectively. The third interval was used to check the relation $t(\mu,f) + t(f,e) = t(\mu,e)$. During the measurements, less than 1% of triple events did not satisfy this condition and were rejected in the off-line analysis.

Typical count rates in the three distributions were a few s^{-1} for (μ,f), about 1500 s^{-1} for (μ,e), and less than 1 s^{-1} for (f,e). In order to avoid distortion in the distributions, events where two electrons occurred within 5 μs of each other were rejected. In addition, all events were tagged with a label according to whether or not a beam particle registered as a (12) coincidence was accompanied by a second particle within a set time limit, normally ±10 μs. "Multi-muon" events were treated as background and could be used to check the effective duty cycle.

Double events (μf, μe, or fe) and triple events (μfe) were recorded. In the case of triple events, the time differences were registered event by event. For double events the time distributions were recorded as histograms which were dumped after the completion of a run. Also in the case of triple events (μfe), histograms were formed, one for each possible projection. The single count rates of the detectors as well as the rates of different coincidences, corrected for the dead-time of the whole system, were recorded with regular intervals during the measurements. In fig. 3 the schematics of the detectors and data acquisition system are given.

2.3 Checks and procedures

The highest rate of muons stopping in the target chamber as measured by the rate of (μ,f) coincidences was obtained with a 4 cm thick graphite moderator.

The five independent sections of the fission chamber were individually tuned with (π,f) coincidences to operate in the plateau region of their bias curves. After amplification, standard timing pulses were obtained from constant fraction discriminators and summed in a logic mixer unit. The timing conditions were set by using generator signals.

The sensitivity of the chamber to be triggered by beam particles was tested by using a dummy chamber, also divided into independent sections, one of which contained no fissile material. In this way it could be established that the beam particles themselves triggered the chamber at a negligible rate, less than 10^{-4} of the corresponding rate of fission events.

In a different section the same dummy chamber was equipped with a ^{252}Cf source, producing about 2000 fission events s^{-1}. Placed in the normal position inside the electron detector, this chamber could be used for background measurements on the electron counter. The latter was found to respond to gamma or neutron radiation accompanying fission events at a rate of typically a few times 10^{-4} per fission event, depending on the threshold level. Adding a second plastic scintillation counter in the electron detector, we could lower the sensitivity to neutral radiation by a factor of 5 to 10 without influencing the efficiency for counting electrons. The over-all detection efficiency for electrons from the beta-decay of

muons bound to fission fragments was measured to be about 25%. The response of the electron detector to neutral radiation, measured as a function of counter thresholds, showed the typical exponential behaviour.

The 1024-channel TDCs (LRS 2228) were calibrated by using an HP electronic counter, type 5345 A, with an error estimated to be 2×10^{-4}. The measured differential non-linearity was equal to $(-2.5 \pm 0.6) \times 10^{-5}$ per channel. Thus the performance of the TDCs introduced negligible uncertainties in the lifetime measurements of the present experiment.

3. DATA ANALYSIS AND RESULTS

As explained above (see section 2.2), the *double* events were recorded in the form of time distribution histograms. The one representing the time distribution μf was used to determine the disappearance rates of muons in thorium and uranium. Standard least squares methods [28] were used to analyse these data. The results have been reported in ref. 13: $\tau = (77.3 \pm 0.3)$ ns for ^{232}Th, and $\tau = (77.1 \pm 0.2)$ ns for ^{238}U (see fig. 4).

Concerning the *triple* events μfe and the correlations established in the analysis of the data, one way of representing these is in the form of a scatter plot with the time difference muon-electron along one axis and the time difference muon-fission along the other. Figure 5 shows such a scatter plot of part of the ^{238}U data. Its characteristic feature is that the events mainly fall on three ridges, two along the coordinate axes, indicating prompt fission (ridge *a*) and prompt "electrons" (ridge *b*), respectively, and the third along the locus for events with fission and "electron" counts in coincidence (ridge *c*). In addition, there are rare events in the two regions

$$\text{(A):}\quad t(\mu,e) > t(\mu,f) > 0 \text{ and}$$

$$\text{(B):}\quad t(\mu,f) > t(\mu,e) > 0\ ,$$

both of which are "physical" regions in the sense that the muon always comes before the other two events (fission and electron). "Non-physical" events appear in the three quadrants where either t(μ,f) or t(μ,e), or both, take negative values.

An ambiguity in the data evaluation procedure stems from the fact that the three prominent ridges merge in the origin of the coordinate system, where $t(\mu,f) = t(\mu,e) = 0$. In order to check the consistency of the interpretation given to the distributions observed along the ridges, events from the area around the origin were redistributed among the three main spectra. In the case of rare events, this difficulty was overcome by not including this area in the analysis.

The redistribution of events between the three ridges was performed with a Monte Carlo method, the weights being defined by the product of two factors: the exponential decay rate along the ridge, and the Gaussian distribution of events in the plane perpendicular to the ridge.

It was found that the following main features of the produced time spectra were quite stable with regard to reasonable changes in the parameters of the exponential and Gaussian distributions:

i) the excess of prompt events belongs to ridge *a*, whereas ridges *b* and *c* are free from such prompt excess events;

ii) there are two components along ridge *c* of approximately equal intensities.

Using the procedure described above, three distributions were obtained. They are shown in figs. 6 to 8 for ridges *a*, *b*, and *c*, respectively.

3.1 Ridge *a*

The distribution for ridge *a* contains events lying in the band -5 ns $< t(\mu,f) <$ $< +5$ ns, projected onto the $t(\mu,e)$ axis. This spectrum was discussed in our previous paper [12]. The uranium spectrum (see fig. 6a) contained two components, one (134 ± 4) ns and the other (1.6 ± 0.4) μs. In the case of thorium (see fig. 6b), where the statistical accuracy was lower, only one component could be discerned, (132 ± 7) ns.

For uranium the relative yield of the longer component is (10 ± 2)%. Taking into account the difference in muon absorption rates as defined by the measured mean lifetimes, it is found that about 1% of all prompt fission events are accompanied by electrons originating from the beta-decay of muons attached to light elements such as hydrogen, carbon, and aluminium, i.e. elements that make up the surroundings of the uranium target.

3.2 Ridge *b*

The distribution shown in fig. 7 contains events for which -8 ns $< t(\mu,e) <$ $< +8$ ns, projected onto the $t(\mu,f)$ axis.

There is no visible prompt part of the distribution, and the disappearance rate is very close to the one measured for the ungated μf spectrum, as presented in fig. 4. The yield of events in this ridge was found to be very sensitive to the threshold settings and the running mode of the electron detector. These observations suggest that the events considered here are due to the detection, by the electron counter, of X-rays from muonic transitions in prompt coincidence with the muon stop, followed by the detection of fission induced by nuclear muon capture.

3.3 Ridge *c*

The distribution shown in fig. 8 contains events lying along the diagonal in the following band:

$$-10 \text{ ns} < t(\mu,f) - t(\mu,e) < +10 \text{ ns} ,$$

projected onto the $t(\mu,f)$ axis. The time spectrum clearly contains two components which were fitted to a sum of two exponentials giving the parameters and errors quoted in fig. 8. The intensities of the two components are comparable. These characteristics are nearly independent of the experimental conditions and the width of the band. On the other hand, the yields of the two components normalized to the yield of the ungated μf histogram depend critically on the effective threshold level of the electron counter.

In order to find out whether charged or neutral particles caused the events along ridge *c*, tests were performed with the second version of the electron detector (see subsection 2.1). The tests were performed i) with the uranium chamber, in the beam; and ii) off beam, with the dummy chamber containing the ^{252}Cf source.

Using the ungated μf histogram as a monitor it was found that in going from the "double" to the "triple" mode of the electron detector, the yield along ridge *a*

remained the same, to within 1%, whereas the yields along ridges *b* and *c* decreased by factors of 2 and 3, respectively.

Furthermore, as was mentioned in section 2.3, it was observed that the number of (fe) coincidences per fission from the ^{252}Cf source was at least five times lower for the triple mode than for the double one. This proves that the overwhelming majority of the events along ridge *c* are caused by neutral radiation detected in the electron counter.

Finally, the number of (fe) coincidences per ^{252}Cf fission event was about the same as the yield of the 80 ns component along ridge *c*, when normalized to the number of ungated μf events.

The significance of these observations will be further discussed in section 4.

3.4 Events outside the ridges

The physical significance of the events falling in regions A and B defined above is schematically described in fig. 9.

In *area A*, where fission precedes the appearance of an electron, we expect to find events due to the spontaneous fission of a muonic shape isomer followed by beta-decay of a muon bound to a fission fragment. In addition, there would be prompt fission events forming a large background in the zero-time region, i.e. along ridge *a*.

In *area B*, where the electron appears before the fission event, the following phenomena would be seen:

i) muon decay followed by spontaneous fission of a shape-isomeric state of the bare nucleus ^{238f}U with a lifetime of (195 ± 30) ns [29];

ii) back-tunnelling to the first well with the corresponding de-excitation gamma-rays giving rise to a signal in the electron detector, followed by fission induced by muon capture.

As is the case for region A, there would be a background; here it would be caused by signals in the electron detector from muonic radiative transitions, i.e. the spectrum along ridge *b*.

In the case where a muonic shape-isomer has been formed as a result of a radiationless transition in the muonic cascade, there are other decay modes possible in addition to the three mentioned above: muon capture or muon decay inducing

fission. Such events would fall on ridge *c* if the neutral radiation accompanying fission triggers the electron counter. In the search for the other three types of events, namely those belonging to regions A and B, the diagonal constitutes a source of background which should be reduced to a negligible amount by a proper choice of limits of the regions where the search is made.

Four spectra obtained for ^{238}U when projecting events from areas A and B onto both axes, t(μ,f) and t(μ,e), are shown in figs. 10 to 13. The events were selected from bands in the scatter plot, shown as inserts on each projection. Using these bands it could be shown that the contribution from the tails of the ridges *a*, *b*, and *c* were made negligibly small. In addition, the random background was sampled by including areas where either t(μ,f) or t(μ,e), or both, were negative. The four distributions will be further discussed in the next section.

3.5 Background events

Regarding the time distributions of background events it was found that the events for which both t(μ,f) and t(μ,e) are negative give random distributions. This is also the case for the events in the second and fourth quadrants when projected onto the axes of negative times. However, these latter events when projected onto the axes of positive times yield exponential distributions with mean lives of about 80 ns for the t(μ,f) axis and about 800 ns for the t(μ,e) axis. These lifetimes correspond to the muon capture rates on Th or U and Al, respectively.

4. DISCUSSION

4.1 The muon capture rate

Since the publication of our results on the muon capture rates in ^{232}Th and ^{238}U studied in the fission mode [13], some new results have appeared on these two nuclei as well as on some other actinides, studied in the fission mode [17,18] and neutron mode [15,16]. Table 1 lists all published values for ^{232}Th and ^{238}U.

As seen from Table 1 there are two cases of significant discrepancies between our values and those reported by other groups. One measurement in the neutron mode

for ^{232}Th [15] gives a difference of (2.8 ± 0.7) ns when compared with our results. For ^{238}U, one measurement in the gamma mode [8] gives a difference of (2.0 ± 0.5) ns.

As discussed in our previous paper [13], the measurements in the fission mode are more reliable due to the essential differences in background conditions. It is significant that in both the cases quoted above, the values obtained by methods other than those using the fission signature are higher. This can be understood by the fact that, whether the background in the other modes of measurement is caused by muons captured by lighter elements in the target region or by muons attached to prompt fission fragments, the measured lifetimes will appear larger than in the case where the fission signal is observed.

However, it is not possible to explain the whole difference by contamination from fission fragments. Using published values for the probability of muon-induced fission and of the ratio between prompt and delayed fission [4,19] for ^{238}U, one obtains a maximum increase of 0.5 ns in the muon lifetime caused by a contribution from muons captured by prompt fission fragments. The remaining discrepancy must be explained by other effects. As remarked in our earlier paper [13], the value of the lifetime was obtained by fitting the experimental data in the time interval 30 to 345 ns. For starting points earlier than 30 ns there was a trend downward for the resulting lifetime. The same effect was observed in the time distribution obtained by the TRIUMF group [17].

4.2 Muon decay after prompt fission

As described in subsection 3.3 above, tests with an improved electron detector confirmed our previous conclusion [12] that ridge a represents triple events with electrons of an energy greater than about 10 MeV. These events could thus only be due to prompt fission induced by radiationless transitions, followed by the beta decay of the muons. By using the so-called Primakoff plot, it could be demonstrated that in most cases the muons become attached to the heavy fragments. From the analysis of the muon-electron time distribution, a 10% fraction of muons attached to the lighter fragments could not be excluded. In a recent paper [16], Schröder et al. report results which support this conclusion. These authors studied muon-induced fission in ^{237}Np, ^{239}Pu, and ^{242}Pu.

Since the publication of our previous report [12], several papers have appeared [24-26,31,32] with theoretical calculations of the probability for the muon to be attached to the light, or heavy fission fragment. In one of the papers [32] only molecular effects, treated in the adiabatic approximation, were considered, whereas other models [24-26] included the dynamics of the fission process. The results range from 1 to 15% for the probability that the muon goes with the light fragment, depending on the model chosen. These studies indicate that an accurate measurement of this probability might yield some information on the nuclear viscosity.

Thus all these calculations give results which, within the quoted accuracy, agree with the experimental upper limit.

For ^{238}U the muon-electron time distribution also contained a long-lived component (see fig. 6), interpreted as being due to muons which have been ejected from a fission fragment and then decay after having been bound to a light nucleus. As discussed in our previous paper [12], the present results on the probability for such a conversion process, together with our observation that muons are predominantly attached to the heavy fragments, are compatible with the theoretical estimates of Barit et al. [33] concerning the muon-conversion probabilities for light and heavy fission fragments. In fact, the correlation between the yield of electrons from converted muons and the conversion probabilities could be used to determine the probability for the muon to be attached to either of the fragments in asymmetric fission.

4.3 Delayed fission

The interaction of negative muons with fissile nuclei can cause delayed fission due to three different processes:

i) nuclear capture of muons;

ii) muon decay; and

iii) population of a fission isomer.

Since in our experiment the electron detector was also sensitive to neutral radiation (muon X-rays, nuclear γ-rays, or neutrons) all three of these processes could be observed. They would be distinguished by the time correlation between fission and "electron" events. The various cases are discussed below, grouped according to the three relations (see scatter plot in fig. 5):

a) $t(\mu,f) - t(\mu,e) = 0$ (ridge *c*)

b) $t(\mu,f) - t(\mu,e) > 0$ (region B)

c) $t(\mu,f) - t(\mu,e) < 0$ (region A) .

4.3.1 Delayed fission simultaneous with "electron" event

Ridge *c*, where the fission chamber and the electron detector are triggered simultaneously, contains two time components (see fig. 8). The longer of these is characteristic of muon capture in the target nuclei. It is interpreted as being due to fission induced by muon capture accompanied by the registration of neutral radiation from the excited fission fragments.

The shorter component in ridge *c*, about 9 ns for both ^{232}Th and ^{238}U, has approximately the same sensitivity to changes in the running conditions of the electron detector as has the longer component in the same ridge, or as have the events in ridge *b* (see section 3.3). We thus conclude that the short component is also produced by neutral radiation in the electron detector, in triple coincidence with muons and fission events. However, from the various tests performed, we are certain that the short component is not due to background from beam pions, or from neutrons produced in the vicinity of the fission chamber. Background caused by tailing from the prompt peak is also excluded.

A different explanation has been tried, based on the possibility of muon transfer from μH, produced by muons stopping in the CH_4 gas of the chamber, to the target nuclei, thorium or uranium. In this case the time modulation would be provided by muon transfer to carbon in the gas, simulating a lifetime of the right order of magnitude.

The fact that this short component is not directly visible in the ungated muon-fission time distribution, whereas in ridge c the 9 ns and 80 ns components have about the same yield, poses great problems for all explanations tried. Some enhancement mechanism must be active when a triple coincidence is required, as for instance a higher gamma energy in the case of the short component. If the muon cascade contains more high-energy X-rays after transfer than in the direct capture in the heavy atom, one might explain why the short component is enhanced. There are other reasons, however, why the explanation using the transfer mechanism meets with difficulties, one of these being the fact that in this case prompt fission should be much more probable than delayed fission due to nuclear muon capture.

By comparing the yield of the longer component with the response of the electron detector to the ^{252}Cf source in the dummy chamber, we have obtained an upper limit for the probability of fission induced by nuclear excitation following muon decay. The yield of prompt fission events (ridge a) in the same ensemble of data was used for normalization. To calculate the upper limit, one further needs the probability of prompt fission per stopped muon. For the two extreme values published for the latter quantity $(1.1 \pm 0.2)\%$ [13], and $(0.23 \pm 0.05)\%$ [4], the upper limit becomes 10^{-2} and 2×10^{-3}, respectively.

The theoretical estimates for the probability of nuclear excitation accompanying muon decay [34] are at least one order of magnitude smaller than the experimental upper limit.

4.3.2 Delayed fission preceded by "electron" event

For area B where the fission event comes after the event in the electron detector, the two projections are presented in fig. 10 and fig. 11. The projection onto the t(μ,e) axis (fig. 10) shows a slight excess beyond the prompt peak.

Figure 11 gives a projection onto the t(μ,f) axis of the events in the interval 10 ns < t(μ,e) < 32 ns. Rough estimates of the yield of the shorter of the two

components present make it plausible that this has a dominant contribution from the tail of ridge *b*. This implies that we see very few events due to back-tunnelling from the second well. It is to be expected that the electron detector is much less sensitive to the gamma radiation from back-tunnelling than from the higher energy X-rays in the muonic cascade.

The few events seen in fig. 11 for t(μ,e) larger than 200 ns are particularly interesting. They cannot be attributed to random background: for negative values of t(μ,f) no single event was recorded for a strip 130 ns long and 20 ns wide. The only explanation for the observed events in fig. 11 seems to be that they are produced by muon decay from the isomeric state, followed by fission from the fission isomer in the bare nucleus. This would be consistent both with the excess at short times in fig. 10 and a possible long component in fig. 11.

If the excess events are considered as an indication that the fission isomer has been populated, they correspond to a probability for such a population of (10 ± 5)% per radiationless muonic transition in ^{238}U. This value was obtained using the probability of muon-induced fission reported in ref. [4] and it is in agreement with the one given in ref. [9]. If the nuclear excitation is due to a radiationless transition process 2p → 1s which has an energy intermediate between the two barriers, as modified by the presence of the muon, one may speculate that the isomeric ratio might resemble the values of Γ_f/Γ for near-barrier photofission of heavy nuclei, i.e. approximately 20%.

4.3.3 Delayed fission followed by an "electron" event

In area A of the scatter plot the fission occurs before the "electron" event. There one would expect to find triple coincidences due to the population of fission isomers which decay by spontaneous fission followed by the beta decay of a muon attached to a fission fragment. Figures 12 and 13 show the projection of these events onto the t(μ,f) and t(μ,e) axes, respectively.

In fig. 12 some excess of events over the background and prompt coincidence curve taken from the measurements with π^- is observed. The events in the interval 8 ns ≤ t(μ,f) ≤ 28 ns are projected onto the t(μ,e) axis in fig. 13. They

are seen to give a distribution which closely resembles the distribution of events along ridge *a*. It is important to realize that the two projections give different time distributions: in this way one can be certain that the excess of events just outside the prompt peak is not a spillover from the much more intense short component in ridge *c*.

Thus we can conclude that region A also gives a weak indication that the fission isomer has been populated and that in muonic atoms the lifetime is considerably shorter than in the bare nucleus. However, for both regions, A and B, the statistical accuracy is too low to draw definite conclusions about the characteristics of the isomeric state. Indications of a short lifetime for the shape isomer in muonic atoms was previously reported to have been observed by Fromm et al. [9] in an experiment searching for back-tunnelling gamma rays. The theoretical calculations by Leander and Möller [21] also point in the direction of a shortened lifetime for the fission isomer in muonic atoms.

Thus until now there is no *conclusive* experimental evidence that the fission isomers are populated in muonic atoms when excited by radiationless muonic transitions.

Acknowledgements

We appreciate very much the assistance of V. Kuznetsov and V.V. Popov in the early stages of the work, as well as the skilful help of J. Tissold during the preparatory stages at CERN. The help given to us by the On-line Data Handling Group, CERN, particularly E. Rimmer and P. Scharff-Hansen in setting up the data acquisition system, was of great importance for the smooth running of our experiment.

We are very much indebted to the staff of the CERN Synchro-cyclotron for reliable and smooth operation of the accelerator and other facilities. Illuminating discussions with A. Bertin, T.E.O. Ericson, G. Ewan, R.A. Eramzhyian, G. Fiorentini, the late S.G. Nilsson, L.J. Ponomarov, J. Rafelski and G. Torelli were of great help

to us. One of the authors (T.K.) acknowledges the hospitality and financial support of the CERN Experimental Physics Division. One author (S.M.P.) is grateful to the Niels Bohr Institute, Copenhagen, for support and for the great hospitality extended to him. Another author (L.W.) is indebted to the Norwegian Research Council for Science and the Humanities for financial support.

REFERENCES

[1] J.A. Diaz, S.N. Kaplan and R.V. Pyle, Nucl. Phys. 40 (1963) 54.

[2] V. Cojocaru, L. Marinescu, M. Petrascu, G. Vioculescu, A. Ignatenko and M. Omelianenko, Phys. Lett. 20 (1966) 53.

[3] B. Budick, S.C. Cheng, E.R. Macagno, A.M. Rushton and C.S. Wu, Phys. Rev. Lett. 24 (1970) 604.

[4] D. Chultem, V. Cojocaru, Dz. Ganzorig, Kim Si Chwan, T. Krogulski, V.D. Kuznetsov, H.G. Ortlepp, S.M. Polikanov, B.M. Sabirov, U. Schmidt and W. Wagner, Nucl. Phys. A247 (1975) 452.

[5] B.M. Aleksandrov, G.V. Buklanov, W.D. Fromm, Dz. Ganzorig, A.S. Krivokhatski, T. Krogulski, S.M. Polikanov and B.M. Sabirov, Phys. Lett. 57B (1975) 238.

[6] Yu. K. Gavrilov, Kim Si Chwan, V. Cojocaru, T. Krogulski, V.D. Kuznetsov, H.G. Ortlepp and S.M. Polikanov, Yad. Fiz. 24 (1976) 241.

[7] O. Hashimoto, S. Nagamiya, K. Nagamine and T. Yamazaki, Phys. Lett. 62B (1976) 233.

[8] S.N. Kaplan, J.A. Monard and S. Nagamiya, Phys. Lett. 64B (1976) 217.

[9] W.D. Fromm, H.-G. Ortlepp, S.M. Polikanov, U. Schmidt, G.N. Zorin, R. Arlt and G. Musiol, Nucl. Phys. A278 (1977) 387.

[10] Dz. Ganzorig, P.G. Hansen, T. Johansson, B. Jonson, J. Konijn, T. Krogulski, V.D. Kuznetsov, S.M. Polikanov, G. Tibell and L. Westgaard, Contribution Q12 to the 7th Int. Conf. on High-Energy Physics and Nuclear Structure, Zürich, Switzerland, 1977.

[11] M.W. Johnson, W.U. Schröder, J.R. Huizenga, W.K. Hensley, D.G. Perry and J.C. Browne, Phys. Rev. C 15 (1977) 2169.

[12] Dz. Ganzorig, P.G. Hansen, T. Johansson, B. Jonson, J. Konijn, T. Krogulski, V.D. Kuznetsov, S.M. Polikanov, G. Tibell and L. Westgaard, Phys. Lett. 77B (1978) 257.

[13] Dz. Ganzorig, P.G. Hansen, T. Johansson, B. Jonson, J. Konijn, T. Krogulski, V.D. Kuznetsov, S.M. Polikanov, G. Tibell and L. Westgaard, Phys. Lett. 78B (1978) 41.

[14] P. Baertschi, A. Grütter, H.R. von Gunten, H.S. Pruys, M. Rajagopalan, H.W. Reist and E. Rössler, Nucl. Phys. A294 (1978) 369.

[15] W.W. Wilcke, M.W. Johnson, W.U. Schröder, J.R. Huizenga and D.G. Perry, Phys. Rev. C 18 (1978) 1452.

[16] W.U. Schröder, W.W. Wilcke, M.W. Johnson, D. Hilscher, J.R. Huizenga, J.C. Browne and D.G. Perry, Phys. Rev. Lett. 43 (1979) 672.

[17] S. Ahmad, G.A. Beer, M.S. Dixit, J.A. Macdonald, G.R. Mason, A. Olin, R.M. Pearce, O. Hausser and S.N. Kaplan, Contribution 5B15 to the 8th Int. Conf. on High-Energy Physics and Nuclear Structure, Vancouver, Canada, 1979.

[18] W.W. Wilcke, M.W. Johnson, W.U. Schröder, D. Hilscher, J.R. Birkelund, J.R. Huizenga, J.C. Browne and D.G. Perry, Phys. Rev. C 21 (1980) 2019.

[19] H.W. Reist, A. Grütter, H.R. von Gunten and D. Jost, Contribution to the Int. Symp. on Physics and Chemistry of Fission, Jülich, 1979: IAEA-SM-241/E2.

[20] J.A. Wheeler, Rev. Mod. Phys. 21 (1949) 133.

[21] G. Leander and P. Möller, Phys. Lett. 57B (1975) 245.

[22] H.J. Specht, J. Weber, E. Konecny and D. Heunemann, Phys. Lett. 41B (1972) 43. D. Habs, V. Metag, H.J. Specht and G. Ulfert, Phys. Rev. Lett. 38 (1977) 387.

[23] S.M. Polikanov, Usp. Fiz. Nauk 107 (1972) 685.

[24] P. Olanders, S.G. Nilsson and P. Möller, Phys. Lett. 90B (1980) 193.

[25] Z.Y. Ma, X.Z. Wu, G.S. Zhang, Y.C. Cho, Y.S. Wang, J.H. Chiou, S.T. Sen, F.C. Yang and J.O. Rasmussen, Preprint, Nuclear Science Division, Lawrence Berkeley Laboratory, University of California, Berkeley, USA, 1979.

[26] J.A. Maruhn, V.E. Oberacker and V. Maruhn-Rezwani, Preprint, Physics Division, Oak Ridge Nat. Lab., Oak Ridge, TN, USA.

[27] E. Segrè, Phys. Rev. 86 (1952) 21.

[28] I.N. Silin, FUMILI, LIKELM, CERN Program Library D 510 (1971).

[29] K.L. Wolf, R. Vandenbosch, P.A. Russo, M.K. Mehta and C.R. Rudy, Phys. Rev. C 1 (1970) 2096.

[30] J.C. Sens, Phys. Rev. 113 (1959) 679.

[31] V.A. Karnaukhov, JINR, preprint E1-11560, Dubna (1978).

[32] Yu.N. Demkov, D.F. Zaretski, F.F. Karpeshin, M.A. Listengarten and V.N. Ostrovski, JETP Lett. 28 (1978) 287.

[33] I.Ya. Barit, G.E. Belovitski and D.F. Zaretski, Inst. of Nuclear Research of the USSR Academy of Sciences, Report R-0058, Moscow (1977).

[34] S.G. Nilsson and I. Ragnarsson, private communication.

Table 1

The muon capture mean lifetimes for ^{232}Th and ^{238}U

Mode of registration	Mean lifetimes τ_μ (ns)		Ref.
	^{232}Th	^{238}U	
e		88.0 ± 4	30
	80.4 ± 2.0	81.5 ± 2.0	7
	79.2 ± 2.0	73.5 ± 2.0	11
γ		79.1 ± 0.5	8
		78.6 ± 1.5	9
n	80.1 ± 0.6	78.3 ± 1.0	15
f	74.2 ± 5.6	75.6 ± 2.9	1
		74.1 ± 2.8	3
	87 ± 4	76.0 ± 1.0	4
	84.0 ± 4.5		6
		77.9 ± 0.5	18
	78.5 ± 2.0	77.7 ± 0.6	19
		76.0 ± 1.3	17
	77.3 ± 0.3	77.1 ± 0.2	this work

Figure captions

Fig. 1 : Schematic view of the apparatus used in the experiment. The muon telescope consists of the plastic scintillation counters C_1-C_3 and a plexiglas Čerenkov counter, $\check{C}$. The graphite moderator, C, is placed between C_2 and $\check{C}$. The electron counter consists of two cylindrical plastic scintillation counters and four plexiglas Čerenkov counters (replacing the previously used H_2O tank).

Fig. 2 : Performance of the fission chamber as measured with the π^- beam:

a) Bias curve of one section of the fission chamber. The arrow indicates the threshold used during the data collection. It corresponds to a fission chamber efficiency of (38 ± 4)% as measured for spontaneous fission of ^{238}U.

b) The time distribution for π^- induced fission events registered in coincidence with the signal from the electron counter.

Fig. 3 : Schematics of detectors, electronics, and data acquisition system.

Fig. 4 : Time distribution of fission events relative to the time of the μ-stop for a) ^{232}Th and b) ^{238}U. The resulting mean lifetimes were obtained by fitting the experimental data in the time interval 30 to 345 ns.

Fig. 5 : Scatter plot of part of the data for μfe triple coincidences. The data fall mainly on the three ridges, corresponding to the following time relations: t(μ,f) = 0 (ridge *a*), t(μ,e) = 0 (ridge *b*), and t(μ,f) = t(μ,e) (ridge *c*). The time range in the t(μ,e) direction is close to 10 times larger than in the t(μ,f) direction.

Fig. 6 : Time distribution of events with the absolute value of t(μ,f) less than 5 ns projected onto the t(μ,e) axis. The experimental data for ^{238}U, fig. 6a, were fitted with the sum of two exponentials and a constant background. In the case of ^{232}Th, fig. 6b, owing to less statistics, only one time component was obtained.

Fig. 7 : Time distribution of events with the absolute value of $t(\mu,e)$ less than 8 ns projected onto the $\tau(\mu,f)$ axis. The decay closely resembles that observed for the ungated (μ,f) time distribution of fig. 4. However, in this case no prompt peak is observed.

Fig. 8 : Time distribution of events with the absolute value of $t(\mu,f) - t(\mu,e)$ less than 10 ns projected onto the $t(\mu,f)$ axis. The experimental data were fitted with the sum of two exponentials and a constant background.

Fig. 9 : Description of the physical significance of events falling in the two regions A and B, characterized by

$$A: \quad t(\mu,e) > t(\mu,f) > 0$$

$$B: \quad t(\mu,f) > t(\mu,e) > 0 \ .$$

In the upper part of the figure the double-humped fission barriers for the muonic atom (solid curve) and for the bare nucleus (dashed curve) are schematically shown. If the nucleus is excited in a radiationless muonic transition it either fissions promptly or decays to the second well. In the latter case the different modes for its subsequent decay are indicated with a reference to the two-dimensional presentation of the time correlation between the fission event and the signal from the electron detector.

Fig. 10 : Projection onto the $t(\mu,e)$ axis of some events from area B for ^{238}U. The shape of the prompt peak was obtained from γ and π^- measurements. The events in the interval 10 ns $< t(\mu,e) <$ 32 ns are projected onto the $t(\mu,f)$ axis in fig. 11.

Fig. 11 : Projection onto the $t(\mu,f)$ axis of some of the events shown in fig. 10. In addition to an exponential corresponding to a lifetime of about 80 ns, there are some events at longer times.

Fig. 12 : Projection onto the $t(\mu,f)$ axis of some events from area A for ^{238}U. The prompt peak drawn as a solid line in the time distribution was

obtained from π^- measurements. The events in the interval 8 ns < < t(μ,f) < 28 ns are projected onto the t(μ,e) axis in fig. 13.

Fig. 13 : Projection onto the t(μ,e) axis of some of the events shown in fig. 12. After correction for the long component visible in the interval 500 to 800 ns, the contents of the channels were added five by five, giving the four points in the interval 0 to 400 ns. Also shown in the decay curve characteristic of prompt fission events from ridge α. The two distributions are seen to be very similar.

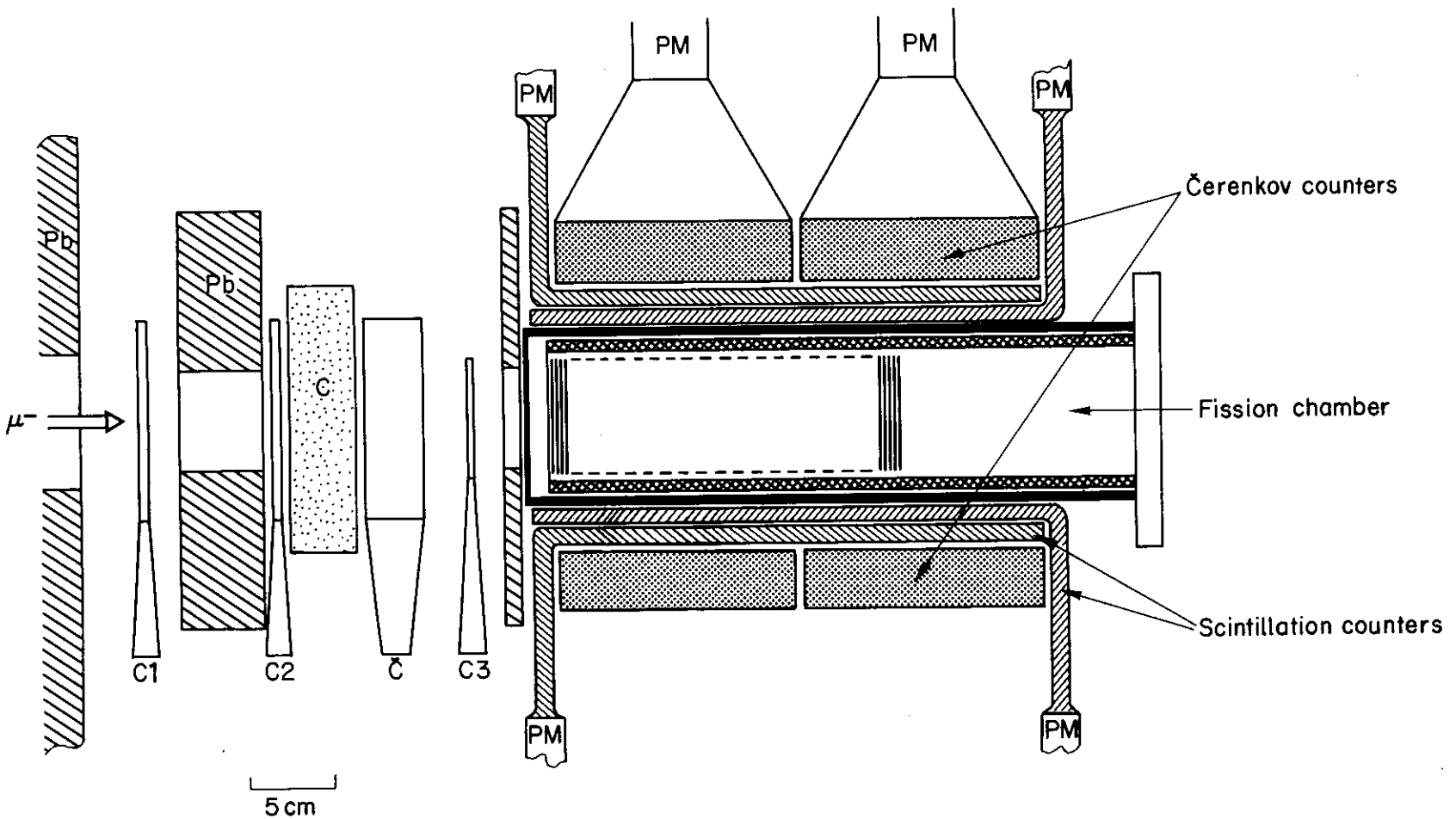
Pb
Pb
C
μ⁻
C1
C2
Č
C3
5 cm
PM
PM
PM
PM
PM
PM
Čerenkov counters
Fission chamber
Scintillation counters

Fig. 1

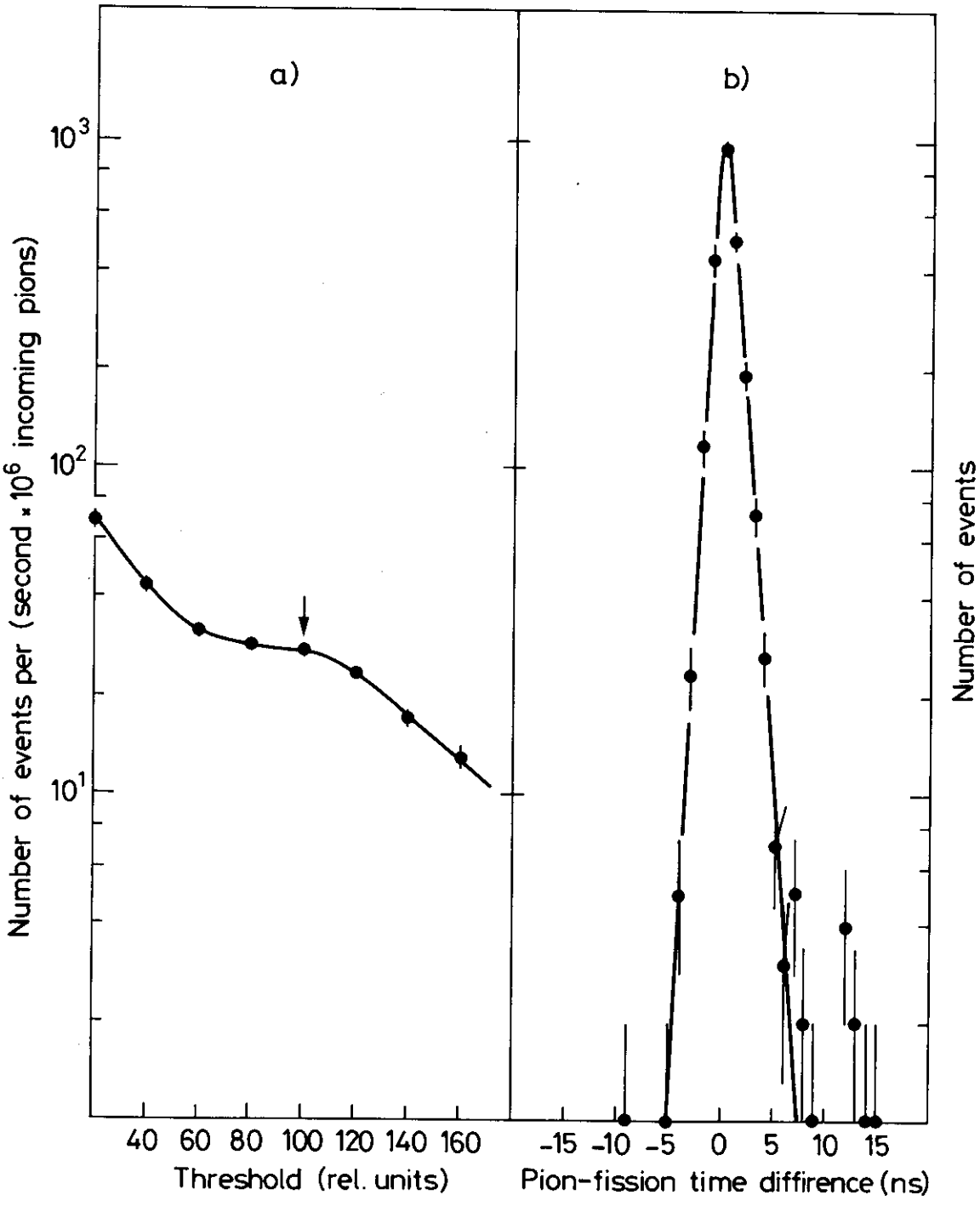
a)
b)
10^3
10^2
10^1
Number of events per (second * 10^6 incoming pions)
Number of events
40 60 80 100 120 140 160
Threshold (rel. units)
-15 -10 -5 0 5 10 15
Pion-fission time diffirence (ns)

Fig. 2

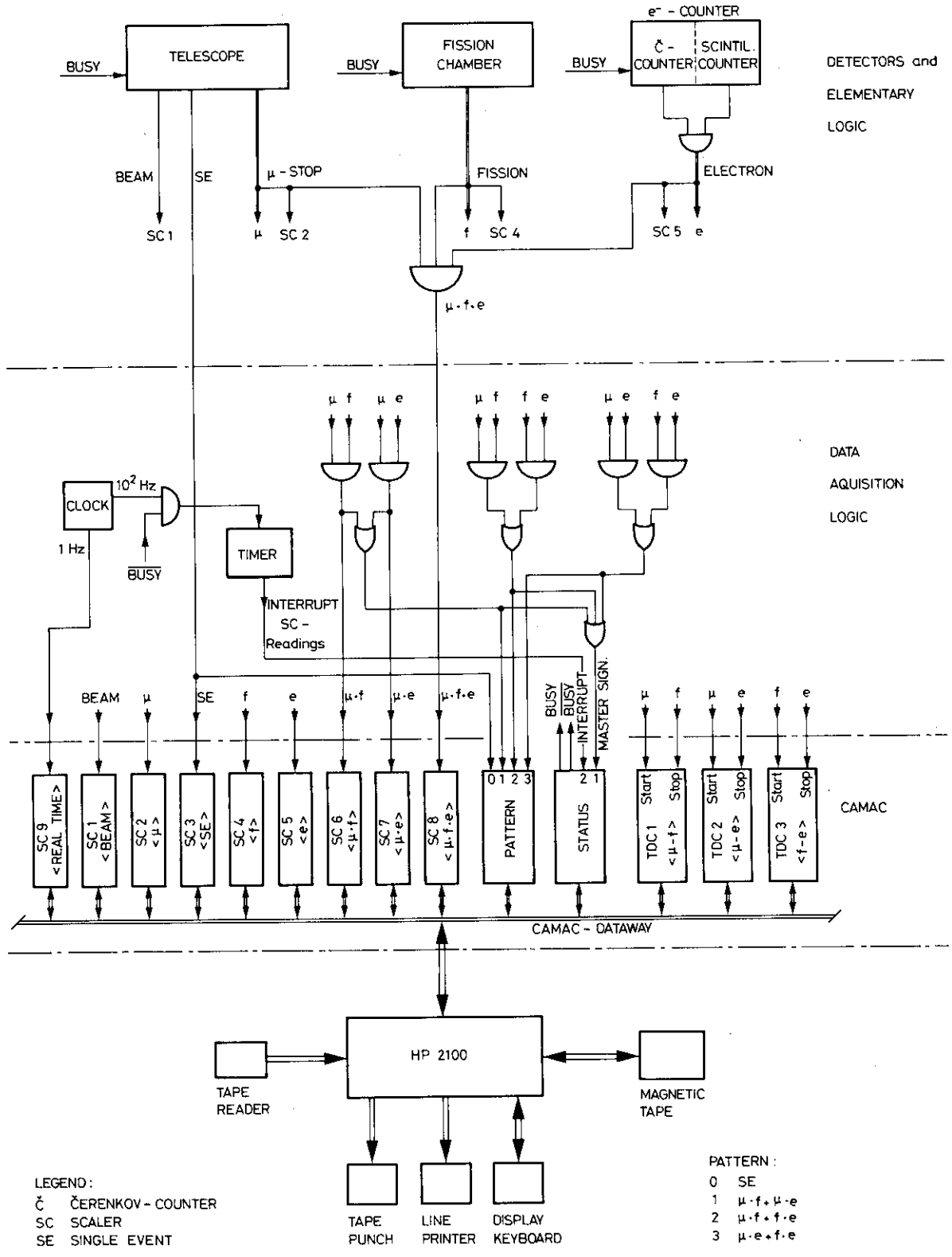
e⁻ - COUNTER
BUSY
TELESCOPE
BUSY
FISSION CHAMBER
BUSY
Č - COUNTER
SCINTIL. COUNTER
DETECTORS and ELEMENTARY LOGIC
BEAM
SE
μ - STOP
FISSION
ELECTRON
SC 1
μ
SC 2
f
SC 4
SC 5
e
μ·f·e
μ f
μ e
μ f
f e
μ e
f e
DATA AQUISITION LOGIC
CLOCK
10² Hz
1 Hz
BUSY
TIMER
INTERRUPT
SC - Readings
BEAM
μ
SE
f
e
μ·f
μ·e
μ·f·e
BUSY
BUSY
INTERRUPT
MASTER SIGN.
μ
f
μ
e
f
e
SC 9 <REAL TIME>
SC 1 <BEAM>
SC 2 <μ>
SC 3 <SE>
SC 4 <f>
SC 5 <e>
SC 6 <μ·f>
SC 7 <μ·e>
SC 8 <μ·f·e>
PATTERN
0 1 2 3
STATUS
2 1
TDC 1 <μ-f>
TDC 2 <μ-e>
TDC 3 <f-e>
Start
Stop
CAMAC
CAMAC - DATAWAY
HP 2100
TAPE READER
MAGNETIC TAPE
TAPE PUNCH
LINE PRINTER
DISPLAY KEYBOARD
LEGEND:
Č ČERENKOV - COUNTER
SC SCALER
SE SINGLE EVENT
PATTERN:
0 SE
1 μ·f + μ·e
2 μ·f + f·e
3 μ·e + f·e

Fig. 3

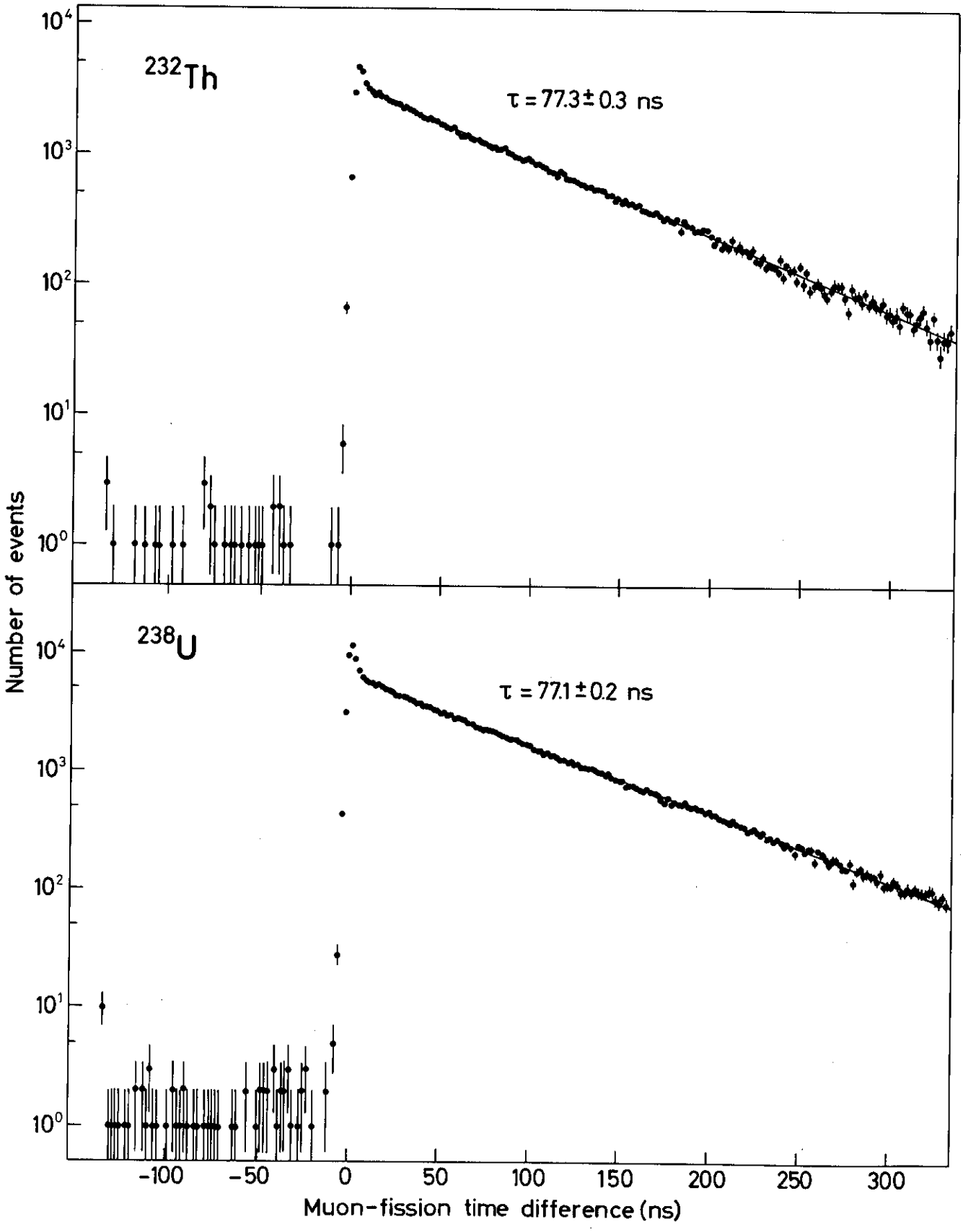
^{232}Th
τ = 77.3 ± 0.3 ns
^{238}U
τ = 77.1 ± 0.2 ns
Number of events
Muon-fission time difference (ns)
10^4
10^3
10^2
10^1
10^0
-100
-50
0
50
100
150
200
250
300

Fig. 4

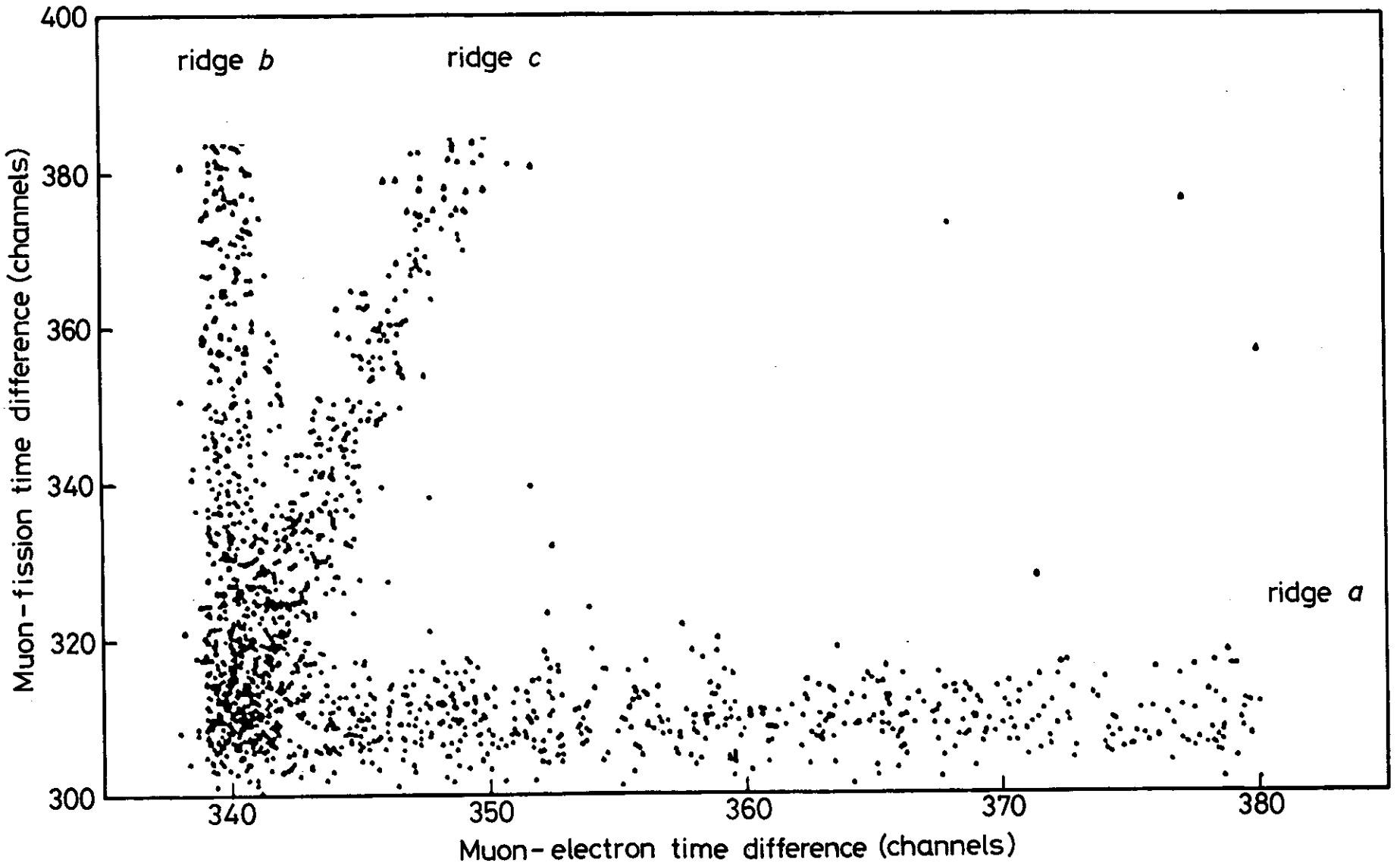
ridge b
ridge c
ridge a
400
380
360
340
320
300
340
350
360
370
380
Muon-fission time difference (channels)
Muon-electron time difference (channels)

Fig. 5

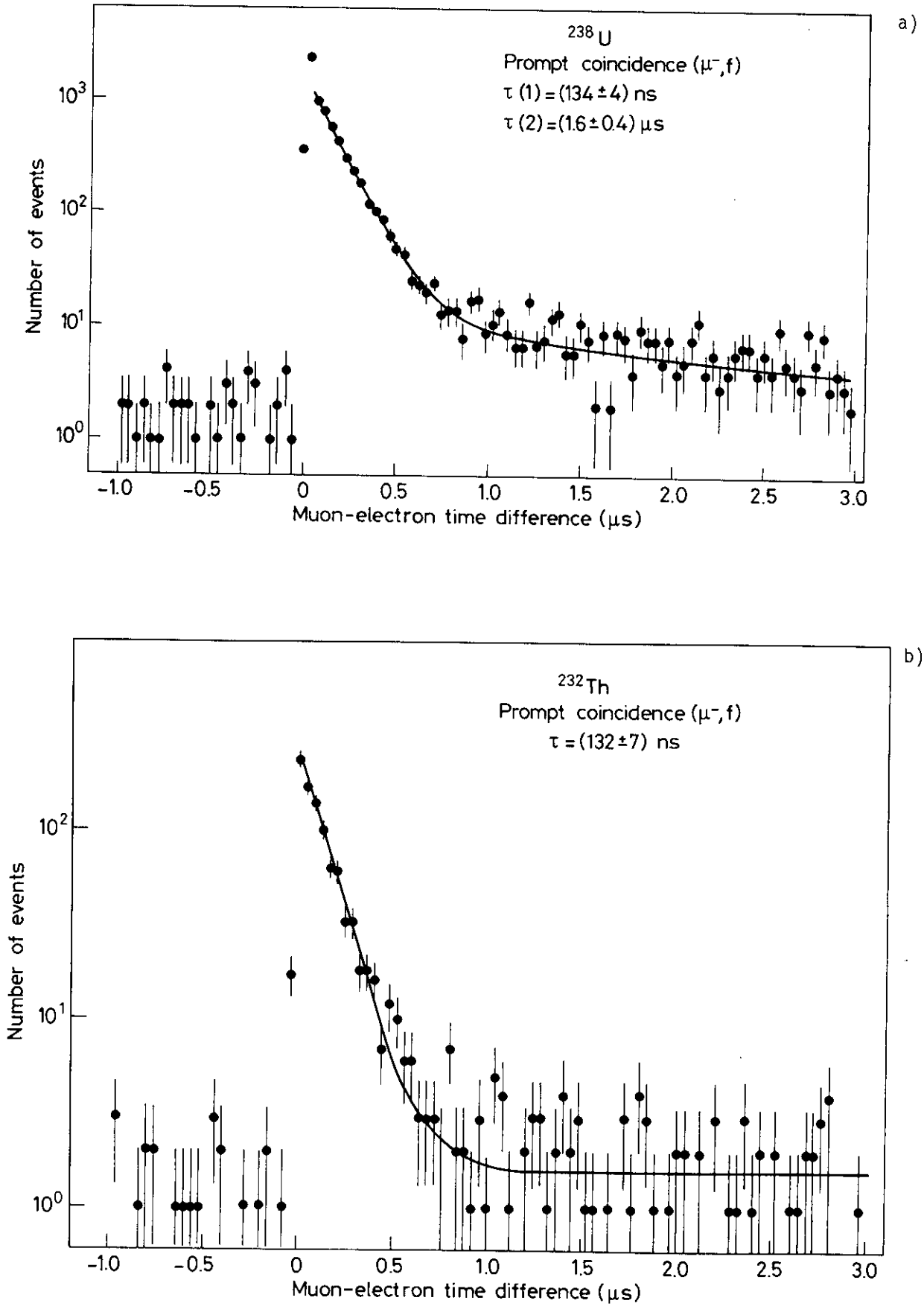
a)
^{238}U
Prompt coincidence (μ^-,f)
τ (1) = (134 ± 4) ns
τ (2) = (1.6 ± 0.4) μs
Number of events
Muon-electron time difference (μs)
b)
^{232}Th
Prompt coincidence (μ^-,f)
τ = (132 ± 7) ns
Number of events
Muon-electron time difference (μs)

Fig. 6

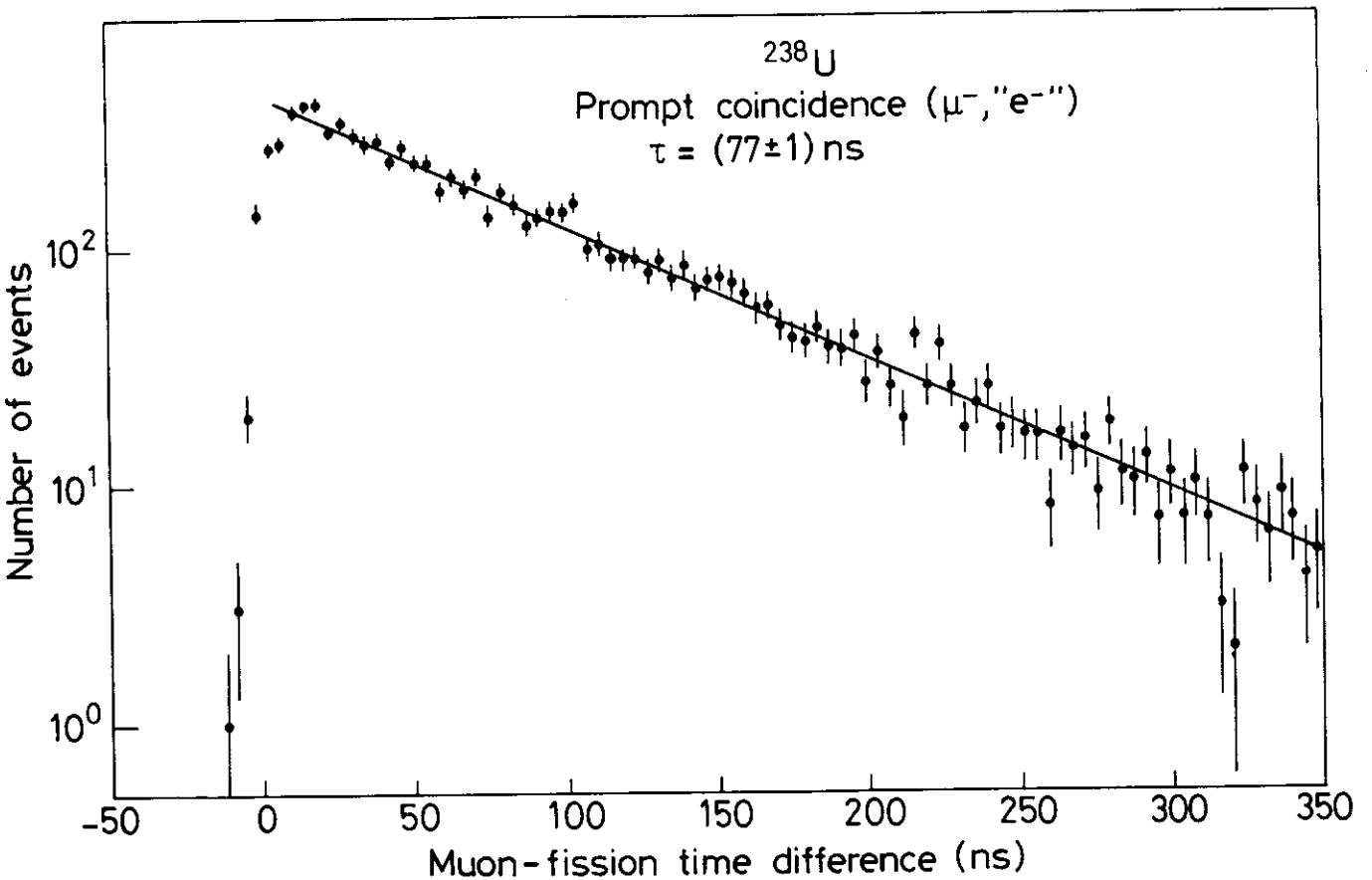
^{238}U
Prompt coincidence (μ^-,"e^-")
τ = (77±1) ns
Number of events
10^2
10^1
10^0
-50
0
50
100
150
200
250
300
350
Muon-fission time difference (ns)

Fig. 7

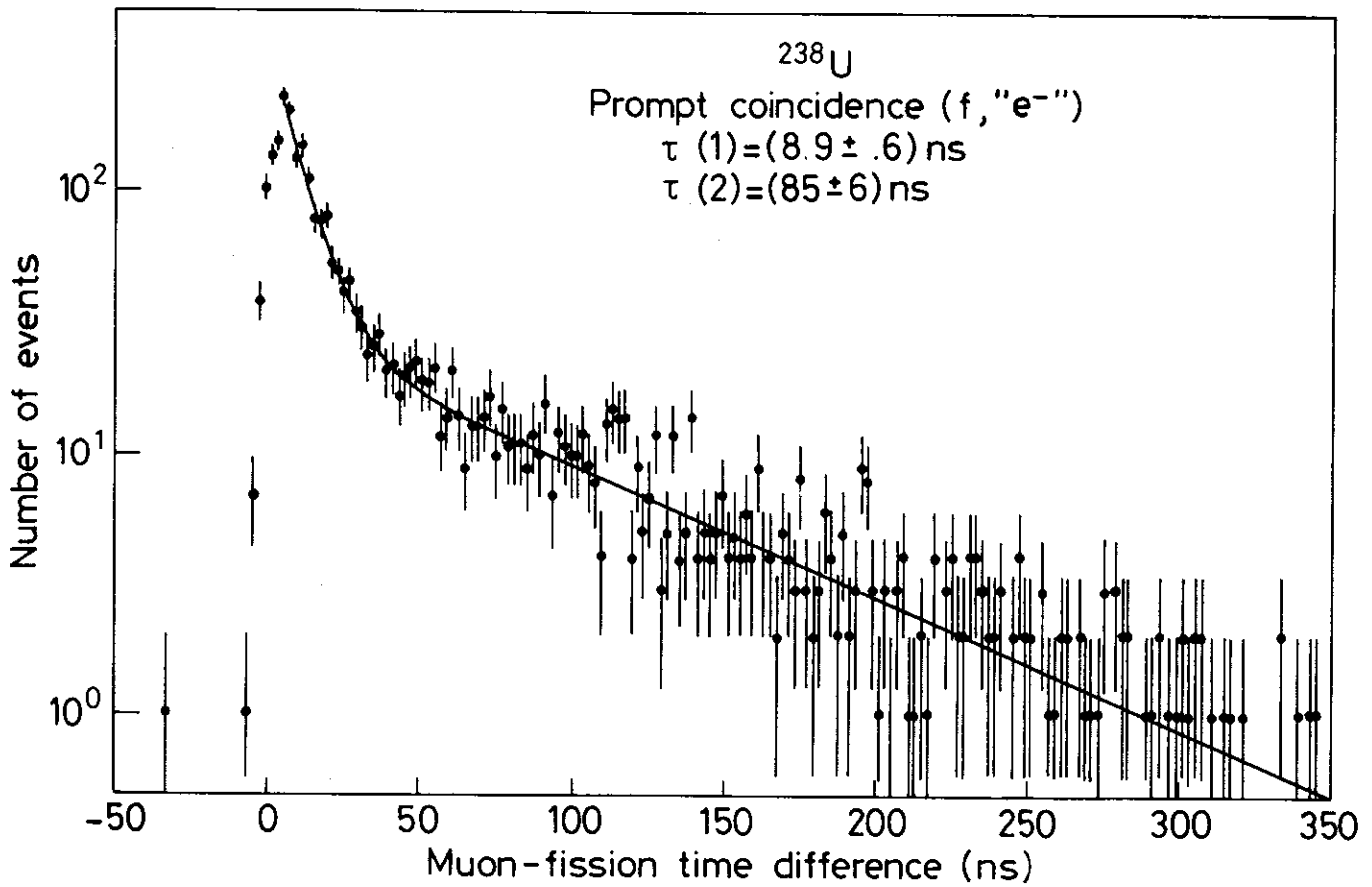
^{238}U
Prompt coincidence (f,"e$^-$")
τ (1)=(8.9± .6) ns
τ (2)=(85±6) ns
Number of events
10^2
10^1
10^0
-50
0
50
100
150
200
250
300
350
Muon-fission time difference (ns)

Fig. 8

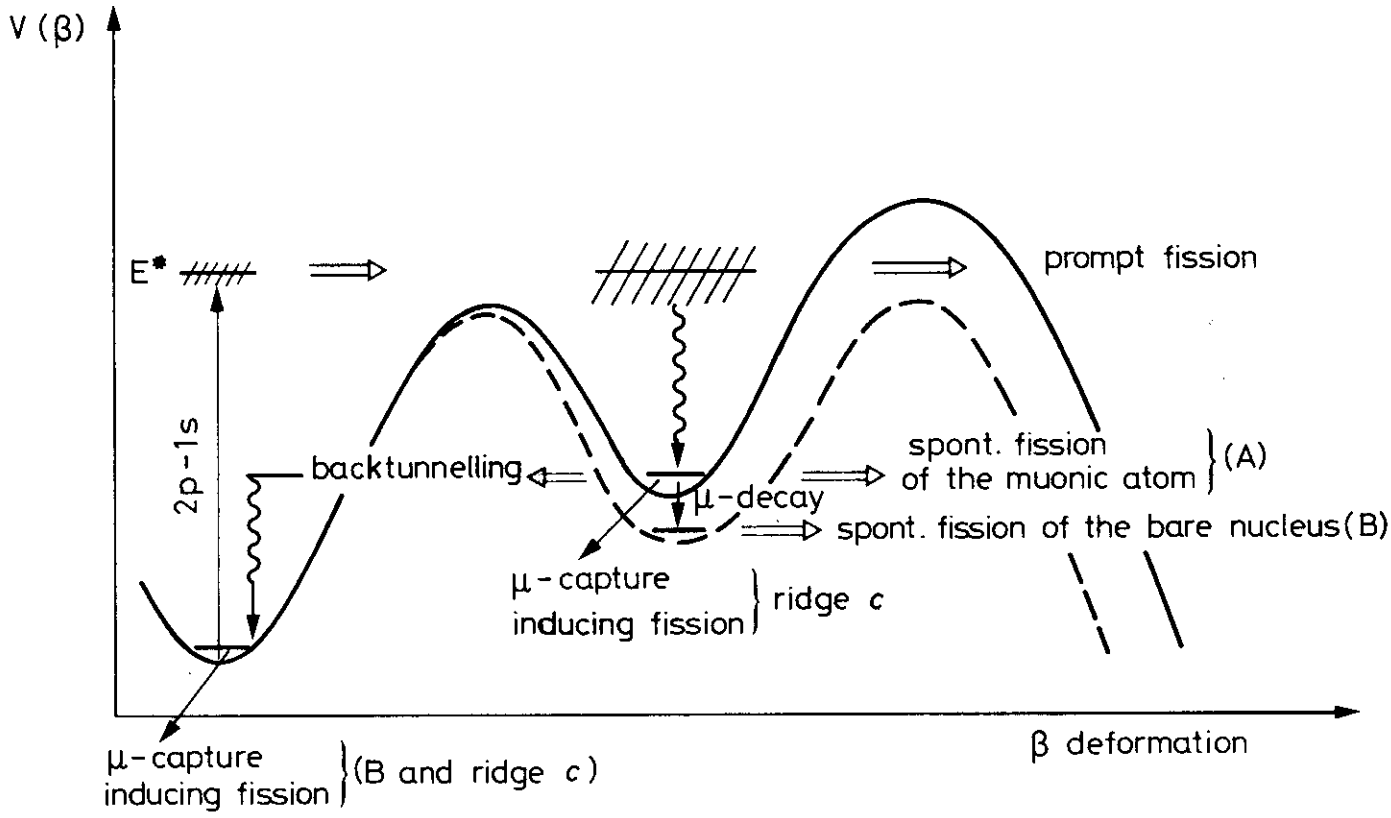
V (β)
E*
2p-1s
backtunnelling
μ-decay
μ-capture inducing fission
ridge c
prompt fission
spont. fission of the muonic atom
(A)
spont. fission of the bare nucleus (B)
β deformation
μ-capture inducing fission
(B and ridge c)

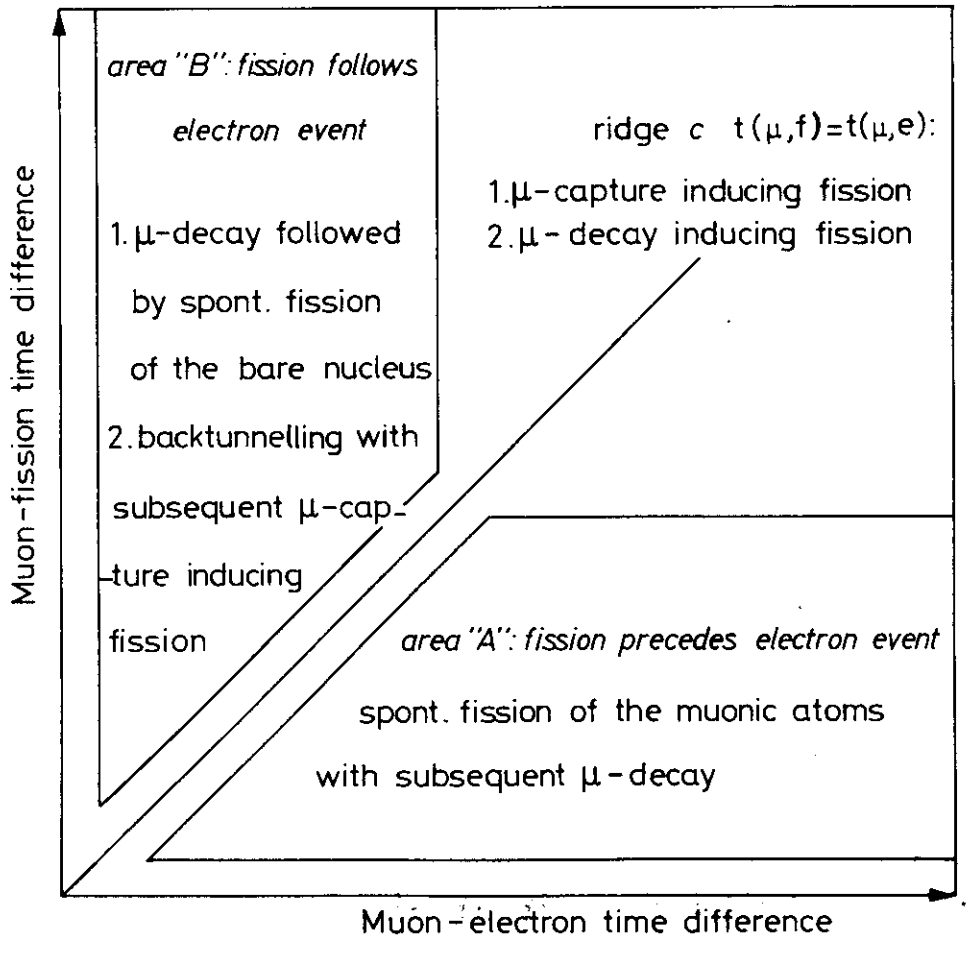
area "B": fission follows electron event
1. μ-decay followed by spont. fission of the bare nucleus
2. backtunnelling with subsequent μ-capture inducing fission
ridge c t(μ,f)=t(μ,e):
1. μ-capture inducing fission
2. μ-decay inducing fission
area "A": fission precedes electron event
spont. fission of the muonic atoms with subsequent μ-decay
Muon-fission time difference
Muon-electron time difference

Fig. 9

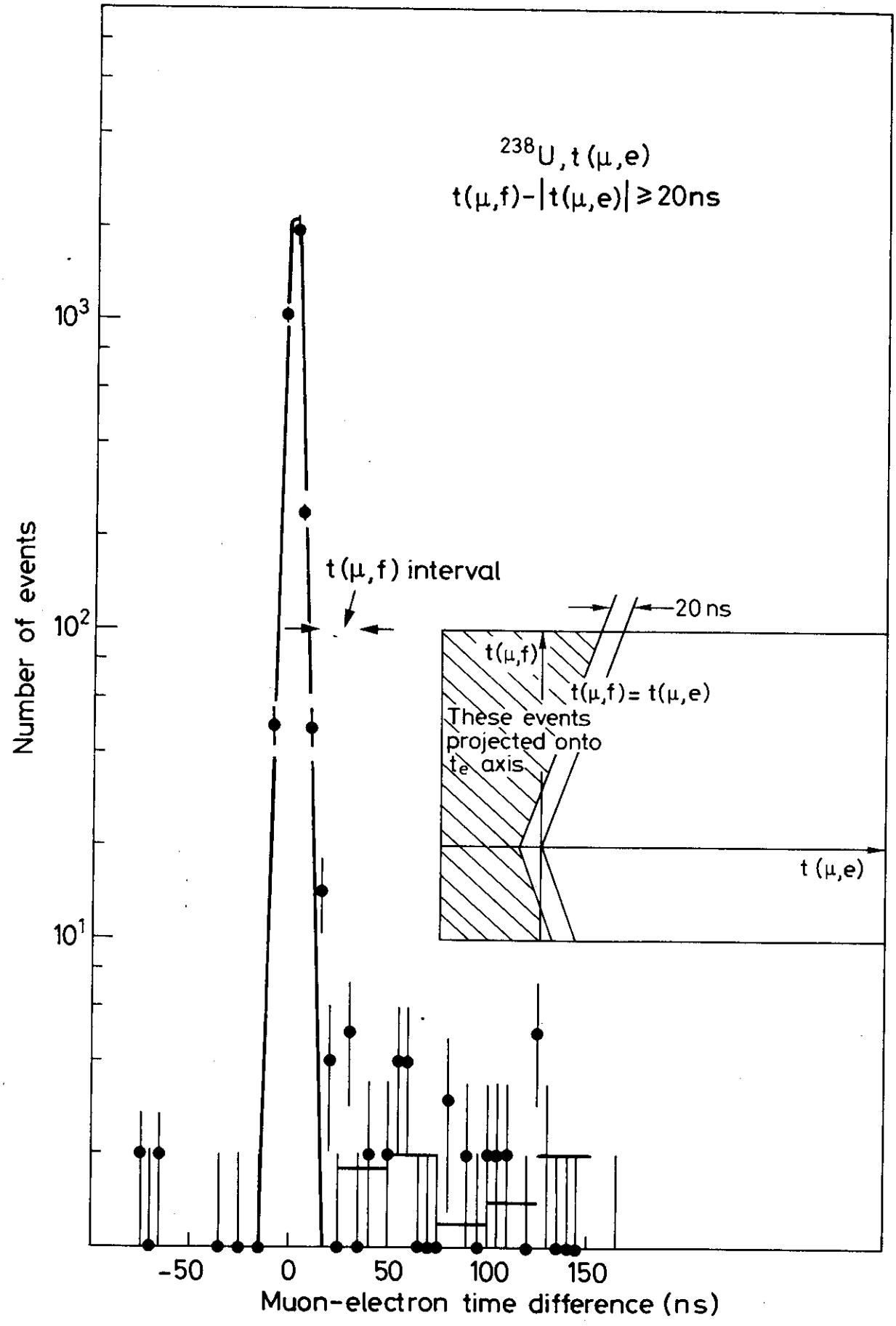
$^{238}U, t(\mu,e)$
$t(\mu,f) - |t(\mu,e)| \geq 20ns$
10^3
10^2
10^1
Number of events
t(μ,f) interval
20 ns
t(μ,f)
t(μ,f)= t(μ,e)
These events projected onto t_e axis
t (μ,e)
-50
0
50
100
150
Muon-electron time difference (ns)

Fig. 10

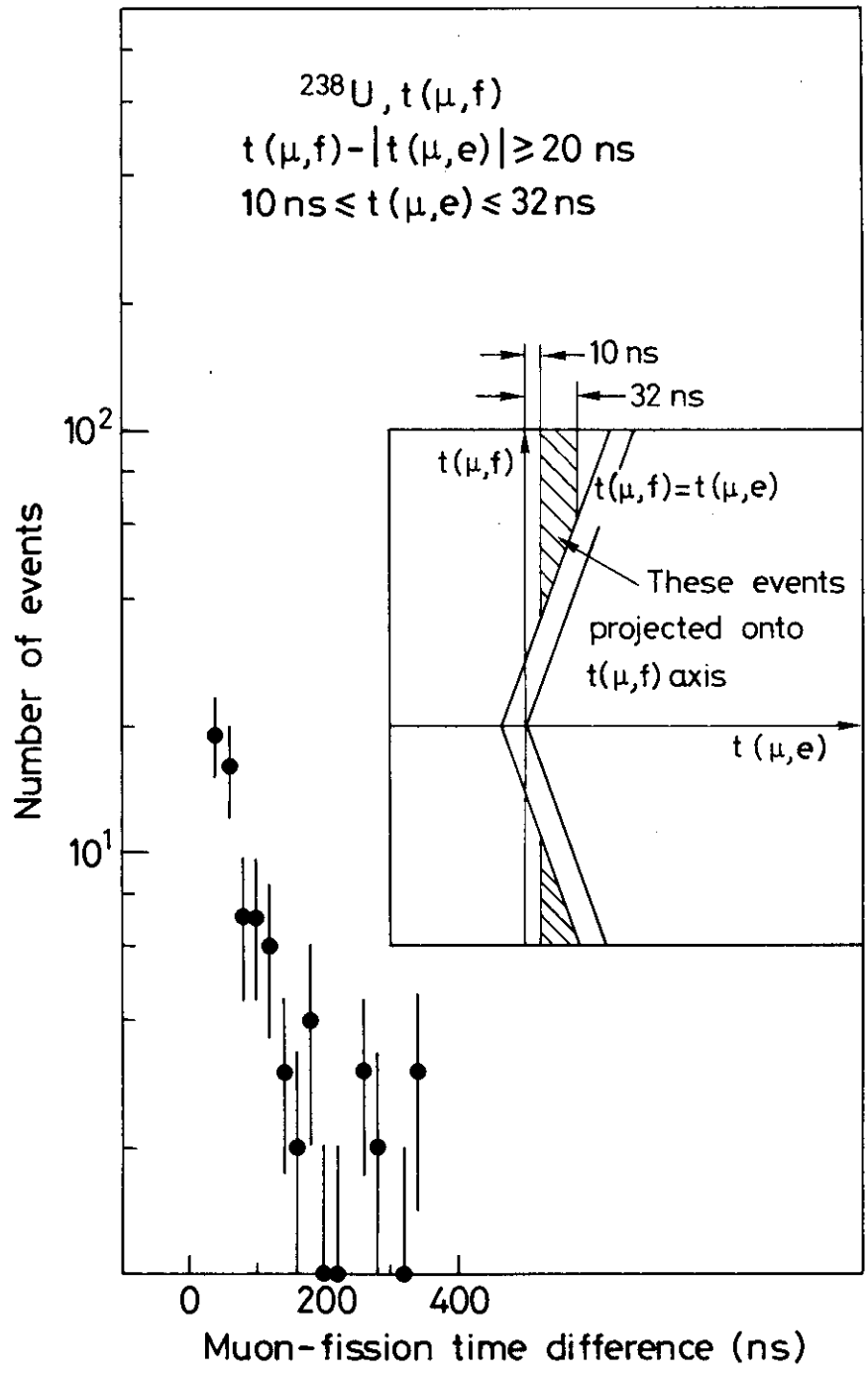
^{238}U, t (μ,f)
t (μ,f) - |t (μ,e)| ≥ 20 ns
10 ns ≤ t (μ,e) ≤ 32 ns
10 ns
32 ns
t (μ,f)
t (μ,f) = t (μ,e)
These events projected onto t(μ,f) axis
t (μ,e)
Number of events
10^2
10^1
0
200
400
Muon-fission time difference (ns)

Fig. 11

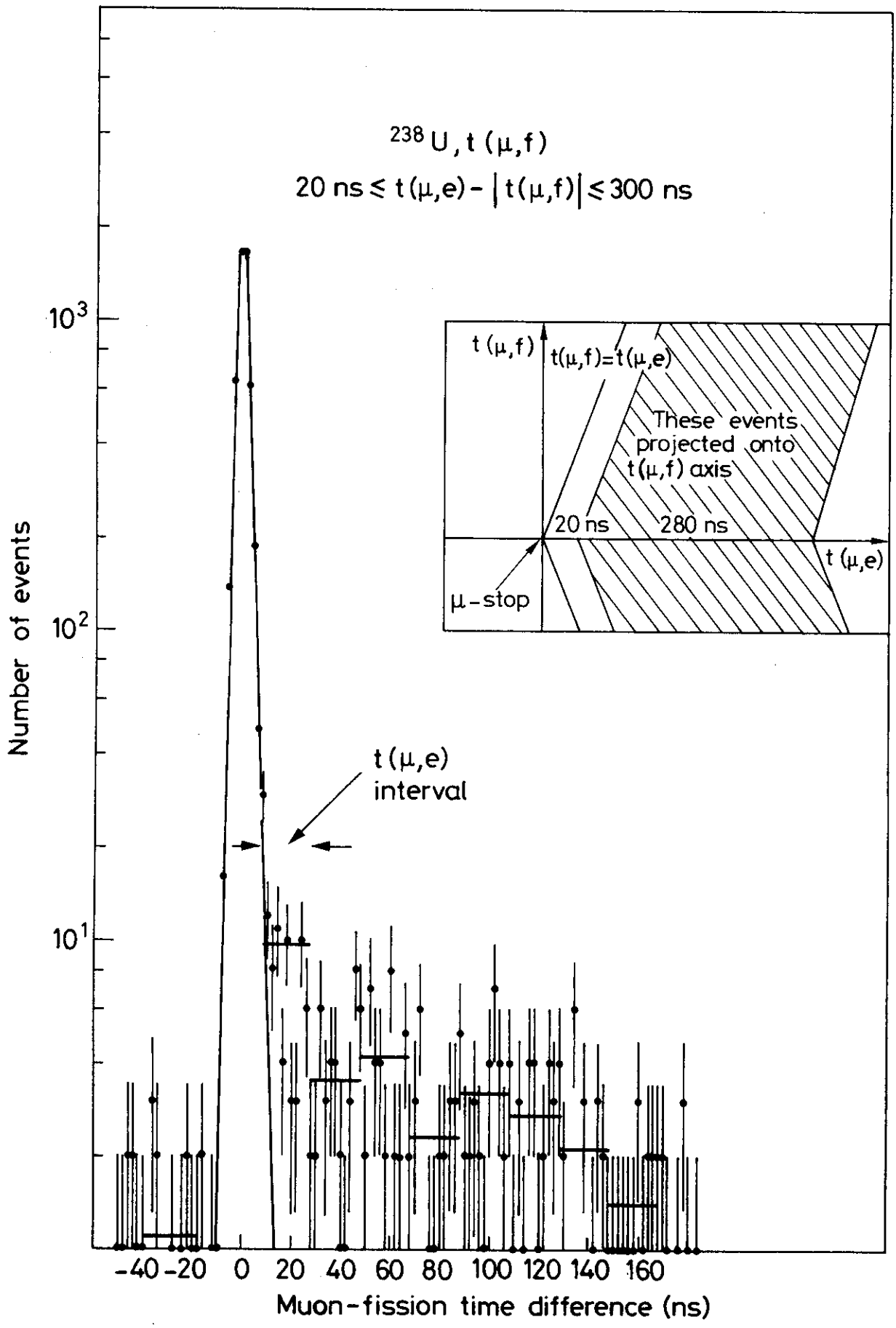
^{238}U, t (μ,f)
20 ns ≤ t(μ,e) − |t(μ,f)| ≤ 300 ns
Number of events
10³
10²
10¹
t (μ,f)
t(μ,f)=t(μ,e)
These events projected onto t(μ,f) axis
20 ns
280 ns
t (μ,e)
μ-stop
t (μ,e) interval
-40 -20 0 20 40 60 80 100 120 140 160
Muon-fission time difference (ns)

Fig. 12

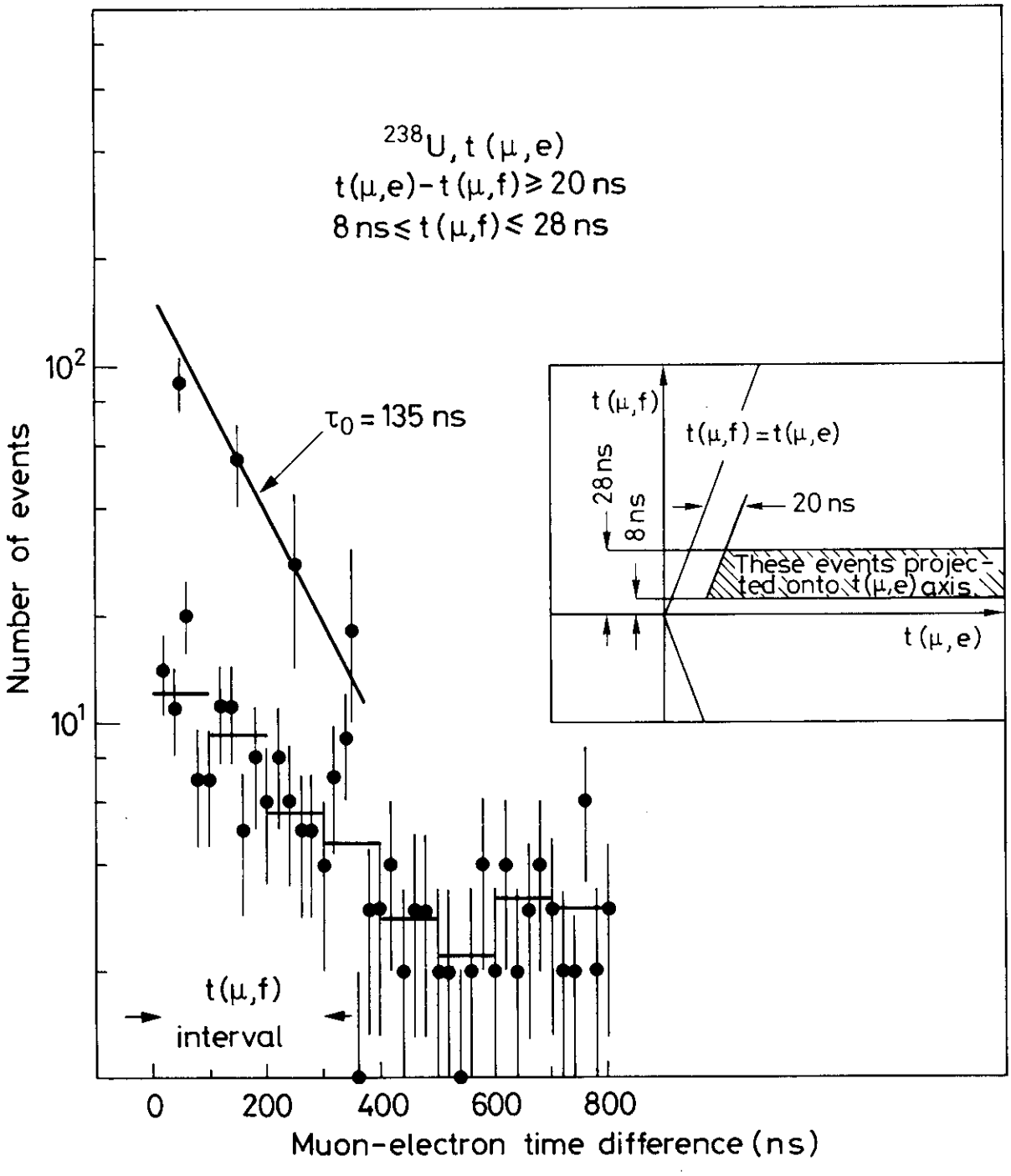
^{238}U, t (μ, e)
t(μ,e) − t (μ,f) ≥ 20 ns
8 ns ≤ t (μ,f) ≤ 28 ns
10^2
10^1
Number of events
τ_0 = 135 ns
t (μ,f)
interval
t (μ,f)
t(μ,f) = t(μ,e)
28 ns
8 ns
20 ns
These events projected onto t(μ,e) axis
t (μ, e)
0
200
400
600
800
Muon-electron time difference (ns)

Fig. 13